Cell, Volume *132*
Supplemental Data

XMAP215 is a processive microtubule polymerase

Gary J. Brouhard, Jeffrey H. Stear, Tim L. Noetzel, Jawdat Al-Bassam,
Kazuhisa Kinoshita, Stephen C. Harrison, Jonathon Howard, and Anthony A. Hyman

1 Legends for supplemental movies

Movie S1 | XMAP215 induced microtubule polymerization (cell3689_mmc2.avi) — A GMPCPP microtubule seed (red) is shown immobilized on a cover glass surface. Microtubule growth occurs by extension from the seed, and the dynamic microtubule lattice is visualized using Alexa Fluor 488 tubulin (green) and TIRF microscopy. Images were recorded with 5 s intervals. The experiment uses Imaging Buffer with 100 nM XMAP215, 4.5 μM unlabeled tubulin, and 0.5 μM Alexa-tubulin (see Methods). The growth rate is 3.0 μm$\cdot$min^{-1}. Video playback is 50$\times$ real-time. A kymograph from this movie is shown in Figure 1B.

Movie S2 | XMAP215 molecules "tip-track" on growing microtubule ends (cell3689_mmc3.avi) — GMPCPP microtubule seeds (red) are shown immobilized on a cover glass surface. 50 nM XMAP215-GFP is introduced, and bright foci of XMAP215-GFP (green) are observed growing from the microtubule seeds by TIRF microscopy. White arrows indicate XMAP215-GFP foci. Images were recorded at 3 s intervals. The experiment uses Imaging Buffer with 50 nM XMAP215-GFP and 5 μM unlabeled tubulin (see Methods). Video playback is 50$\times$ real-time. A kymograph from this movie is shown in Figure 2A.

Movie S3 | Single XMAP215 molecules observed under growth conditions (cell3689_mmc4.avi) — GMPCPP microtubules (red) are shown immobilized on a cover glass surface. Imaging buffer containing 5 nM XMAP215-GFP (green) and 95 nM unlabeled XMAP215 was introduced (see Methods). TIRF images of XMAP215-GFP were recorded in continuous streaming mode with 100 ms exposure time per frame. The streaming movie was overlaid onto one static epifluorescence image of the microtubules. Video playback is in real-time.

Movie S4 | XMAP215 catalyzes both growth and shrinkage of microtubules (cell3689_mmc5.avi) — Timelapse movie of a GMPCPP microtubule seed (red) exposed to 100 nM XMAP215 at 3 tubulin concentrations: 0 μM, 0.1 μM Alexa-tubulin (green), and 0.5 μM Alexa-tubulin and 4.5 μM unlabeled tubulin (see Methods). Images were recorded at 5 s time intervals. Video playback is 50$\times$ real-time. A kymograph from this movie is shown in Figure 5A.

2 XMAP215 increases the association rate constant of tubulin

2.1 XMAP215 promotes plus-end growth

We used polarity-marked microtubules to verify that XMAP215 promotes microtubule growth from the plus-end of the microtubule, as expected (see Figure S1).

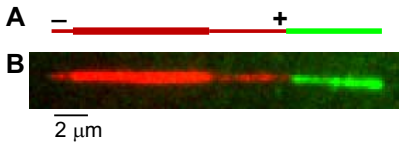

Figure S1: **XMAP215 promotes plus-end growth.** (**A**) Schematic of a polarity-marked GMPCPP microtubule seed (red) with Alexa-tubulin polymerizing from the plus-end. (**B**) Still image corresponding to (A). Image taken in 200 nM XMAP215, 4.5 μM unlabeled tubulin and 0.5 μM Alexa-tubulin. Growth occurs exclusively from the plus end.

2.2 XMAP215 increases the association rate constant by fivefold

The growth of microtubules, meaning the incorporation of tubulin subunits into a microtubule polymer, can be represented thus:

$$\mathrm{T} + \mathrm{T}_n \underset{k_\mathrm{d}}{\overset{k_\mathrm{a}[\mathrm{T}]}{\rightleftharpoons}} \mathrm{T}_{n+1} \tag{S1}$$

where T refers to free tubulin and T_n refers to a microtubule of n tubulin subunits, k_a is the second-order association rate constant, [T] is the concentration of free tubulin, and k_d is the dissociation rate constant of GTP-tubulin. Based on this reaction scheme, the change in the number of tubulin subunits, n, is expressed as:

$$\frac{dn}{dt} = k_\mathrm{a}[\mathrm{T}] - k_\mathrm{d} \tag{S2}$$

The value of dn/dt is measured in the experiment as the change in microtubule length. In order to calculate the association rate constant, it is necessary to know either (a) the growth rate as a function of tubulin concentration, (b) k_d, or (c) the critical concentration where $T_c = k_\mathrm{d}/k_\mathrm{a}$.

We measured the microtubule growth rate as a function of GTP-tubulin concentration in the presence and absence of XMAP215 (see Figure S2). The data indicate a fivefold increase in the association rate constant with 200 nM XMAP215. This measurement agrees with previously published measurements for the growth of GTP-tubulin from microtubule seeds in the presence of XMAP215 (Vasquez et al. 1994) and in the absence of XMAP215 (Drechsel et al., 1992).

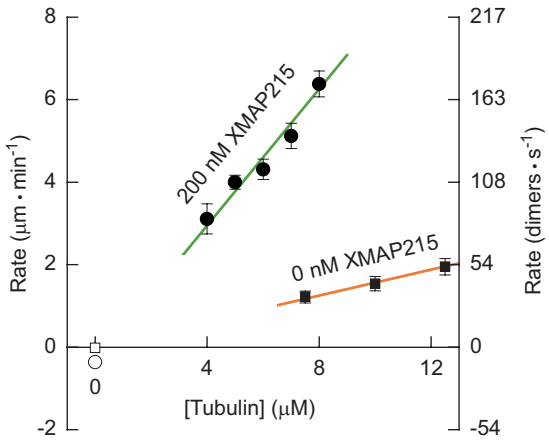

Figure S2: **Microtubule growth rates versus GTP-tubulin concentration in the presence and absence of XMAP215.** Microtubule growth rates were measured in the assay shown in Figure 1. In the presence of 200 nM XMAP215 (black circles), the growth rates increase linearly (green line), indicating an association rate constant of 19.8 $\mu\mathrm{M}^{-1}{\cdot}\mathrm{s}^{-1}$ (assuming 13-protofilament microtubules). In the absence of XMAP215 (black squares), the growth rates also increase linearly (orange line), indicating an association rate constant of 4 $\mu\mathrm{M}^{-1}{\cdot}\mathrm{s}^{-1}$. Error bars represent the SEM ($n \geqslant 10$). The rates at zero tubulin are depolymerization of GMPCPP-tubulin microtubules in the presence (open circle) or absense (open square) of XMAP215. Note that below 4 μM and 7 μM in the presence and absence of XMAP215, respectively, the microtubules do not grow for a long enough time to measure a growth rate.

The treatment above, as expressed in Equation S1, is a simplification. Specifically, modeling microtubule growth in this way does not treat the 13 sites available for tubulin addition individually, but rather is a summation across all 13. Thus the association rate constant per protofilament is only 1/13 that of the whole microtubule.

XMAP215 lowers the minimum concentration of tubulin required to detect growth from microtubule seeds. After this threshold is passed, the microtubule growth rate increases linearly with tubulin concentration, and the slope of this increase extrapolates back to the critical concentration. We chose 5 μM tubulin for most experiments because it is below the threshold for tubulin alone.

3 Behavior of single XMAP215 molecules during microtubule polymerization

Single XMAP215-GFP molecules diffuse on the microtubule lattice and reside for extended periods at the growing microtubule plus end. The distribution of end residence times is shown in Figure 2D.

3.1 The tracked molecules are single XMAP215 monomers

XMAP215 is a monomeric protein. The fluorescent signals we tracked should thus have been XMAP215-GFP monomers. How do we know we are observing single XMAP215 monomers and not aggregated oligomers? Several observations support the argument for single molecules. First, the purified protein eluted from the gel filtration column as a clear, single peak indicative of a homogeneous population. We performed all critical experiments using freshly-purified protein, because freezing has been known to cause aggregation for other proteins. Second, as demonstrated here, electron micrographs of negatively-stained XMAP215 molecules and analytic ultracentrifugation show that XMAP215 is a monomer. These structural and biochemical observations are made at higher XMAP215 concentrations than those used in the single molecule assays, and so we expect even less oligomerization under single-molecule conditions. Third, the GFP signals did not show the two-step bleaching pattern observed for dimeric proteins such as conventional kinesin or MCAK. Rather, the GFP signals simply terminated, either due to dissociation of the molecule or bleaching of the single GFP moeity.

3.2 Correction for photobleaching

The duration of XMAP215-GFP end residence times is observed to decay exponentially (Figure 2D). The observed exponential decay, with a time constant, τ_{obs}, is actually the combination of two processes: (a) the dissociation of XMAP215 from the microtubule and (b) the bleaching of the GFP fluorophore on XMAP215 molecules. The time constants of these two processes are related to the observed time constant by:

$$\frac{1}{\tau_{obs}} = \frac{1}{\tau_B} + \frac{1}{\tau_D} \qquad \text{(S3)}$$

where τ_D is the time constant of XMAP215 dissociation and τ_B is the time constant of bleaching. The time constant of bleaching was measured for stationary XMAP215-GFP molecules that non-specifically adhered to the cover glass surface (Helenius et al., 2006). In the experiment, there are XMAP215-GFP molecules that are irreversibly bound to the cover glass surface, and there are also molecules that transiently interact with the cover glass (0.1-0.2 s) and then dissociate. The number of molecules observed on the surface decayed exponentially as the GFP moieties of the irreversibly-bound molecules bleached (Figure S3), reaching a non-zero plateau. The time constant of bleaching was found to be $\tau_B = 5.55 \pm 0.23$ s for the irreversibly bound molecules, while the plateau value of 50 represents the equilibrium for the transient binding to the cover glass. The time constant of bleaching was used in Equation S3 to calculate τ_D, the mean lifetimes reported in the main text. Errors were propagated in Equation S3 using Maple 9.5 (Maplesoft).

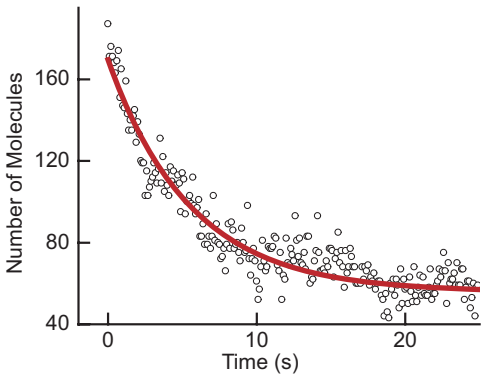

Figure S3: **Timecourse of bleaching for surface-bound XMAP215-GFP molecules.** The number of surface-bound XMAP215-GFP molecules observed (circles) decays exponentially as the GFP moieties are bleached. An exponential decay fit (red line) gives a time constant, τ_B, of 5.55 ± 0.23 s.

4 XMAP215 binds tubulin with 1:1 stoichiometry

We have demonstrated that XMAP215 binds tubulin with a 1:1 stoichiometry by three experimental techniques: analytic size exclusion chromatography, analytic ultracentrifugation, and single molecule microscopy. All three procedures point clearly to a high affinity complex between one tubulin dimer and one XMAP215.

4.1 Size exclusion chromatography

The analytic size exclusion chromatography experiments were repeated at very high tubulin concentration. By adding excess tubulin, we are attempting to force more than one tubulin onto the molecule, to verify that an additional, lower affinity binding site does not exist. Despite increasing the tubulin concentration to 14.3 μM, we do not observe additional tubulin in the complex (Figure S4). The size exclusion chromatography experiments were quantified by image analysis of scanned SDS-PAGE gels.

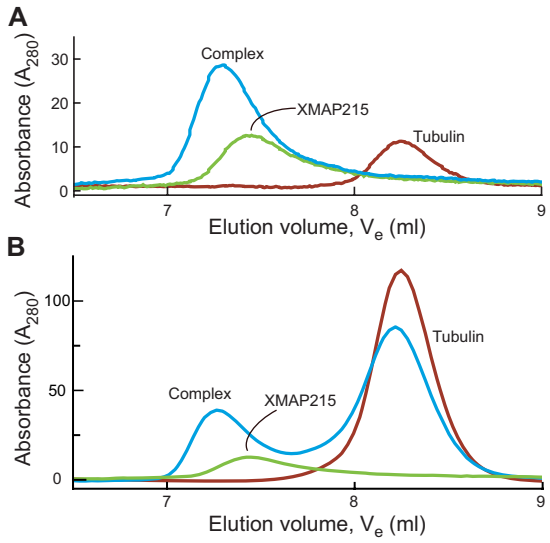

Figure S4: XMAP215 binds tubulin with a 1:1 stoichiometry in the presence of excess free tubulin. The analytic size exclusion chromatography experiments were performed at two XMAP215:tubulin ratios. The elution profiles for tubulin are shown in red, for XMAP215 in green, and for the complex in blue. (**A**) With a ratio of 0.25 tubulins:XMAP215, or 1.43 μM tubulin and 5.75 μM XMAP215, all tubulin is found in complex with XMAP215. (**B**) With a ratio of 2.5 tubulins:XMAP215, or 14.3 μM tubulin and 5.75 μM XMPA215, the binding stoichiometry remains 1:1, with the excess tubulin eluting at its normal V_e.

Table S1: Sedimentation Analysis

Protein	kDa	S_{max}	S	S_{max}/S
Ovalbumin	43	4.43	3.5	1.27
Aldolase	158	10.55	7.3	1.45
Catalase	232	13.63	11.3	1.21
Tubulin	100	7.78	4.7	1.65
XMAP215	229	13.51	6.3	2.14
XMAP215:tubulin	329	17.20	7.9	2.18

4.2 Sedimentation analysis

In order to determine the shape of XMAP215 and the XMAP215:tubulin complex, we measured the sedimentation coefficients for XMAP215 and the XMAP215:tubulin complex using centrifugation in a sucrose density gradient. From these sedimentation coefficients, we calculated the S_{max}/S ratio, which is an indicator of the relative elongation of the molecule (Schurmann et al., 2001). Table S1 shows the measured values including the calibration standards. Both XMAP215 and the XMAP215:tubulin complex have S_{max}/S values that indicate an elongated molecule. In the electron micrographs of negatively stained XMAP215:tubulin complexes, the molecules appear globular, not elongated. The discrepancy indicates that portions of the XMAP215:tubulin complexes are not resolved in the electron micrographs. We hypothesize that the unresolved portion is the C-terminal tail of XMAP215.

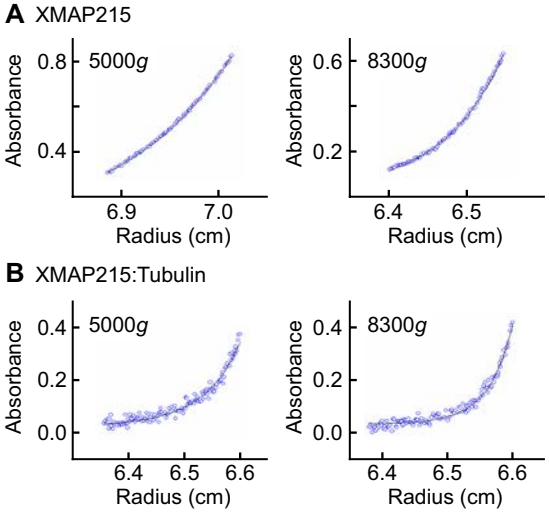

Figure S5: Source data for analytic ultracentrifugation measurements. (A) Plot of absorbance versus radius at 5000 and 8300 g for XMAP215 alone. The fits to the data produce a molecular mass of 220 $\pm$ 10 kDa. (B) Plot of absorbance versus radius at 5000 and 8300 g for XMAP215 + tubulin. The fits to the data produce a molecular mass of 320 $\pm$ 30 kDa. This demonstrates that XMAP215 binds one tubulin dimer.

4.3 Analytic ultracentrifugation

Sedimentation equilibrium analytic ultracentrifugation provides a shape-independent measure of molecular mass. The source data used to determine the mass of XMAP215 and XMAP215:tubulin are shown in Figure S5.

4.4 Quantitative fluorescence of diffusing tubulin

We quantified the fluorescence intensity of the Alexa Fluor 488 tubulin observed in a complex with XMAP215 in the single-molecule fluorescence assay. To do so, we compared the intensity of tubulin bound to the microtubule via XMAP215 with the intensity of surface-bound tubulin observed in the same experiment. As a caveat, the tubulin dimers can carry a variable number of fluorophores, due to the non-specific nature of the chemical labeling, which targeted ε-amine groups on surface lysines. The labeling ratio of the Alexa-tubulin is 0.4, indicating less than one label per tubulin dimer, although this does not exclude dimers with 2 or more fluorophores. This introduces variance in the fluorescence of individual dimers. Additional variance arises from (a) inhomogeneities in the excitation intensity and possibly (b) fluorophore to fluorophore variance due, for example, to the specific residue carrying the label or the orientation of the fluorophore.

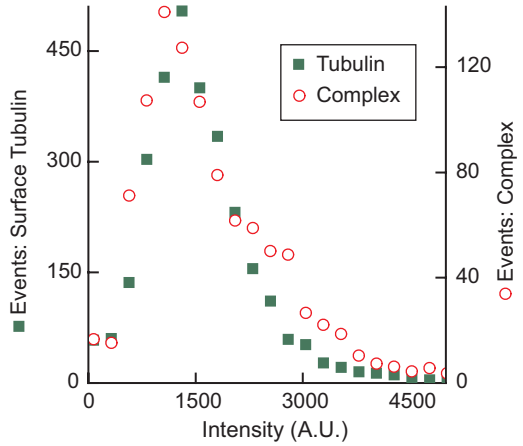

Figure S6: **XMAP215 binds tubulin with a 1:1 stoichiometry on the microtubule lattice.** Histogram of mean intensity values for XMAP215:tubulin complexes on the microtubule lattice (red circles) and surface-bound tubulin dimers in the same experiment (green squares).

These caveats aside, we observe a quantitative fluorescence distribution indicative of single tubulin heterodimers, not oligomers or mini-protofilaments. The intensity values are $I = 1713 \pm 1002$ A.U. for XMAP215:tubulin (mean $\pm$ SD, $n = 962$) and $I = 1542 \pm 761$ A.U. for surface tubulin (mean $\pm$ SD, $n = 2917$). In other words, the mean fluorescence values for XMAP215-bound tubulin differ by <10% from the fluorescence values for surface-bound single tubulins. A histogram of the fluorescence intensity values is shown in Figure S6. The histogram for the complex gives a slight suggestion of a small secondary peak at twice the intensity of the main peak ($I \simeq 3000$). This is likely due to tubulin dimers with two Alexa Fluor 488 labels. This peak may not appear when the tubulin is bound to the surface, due to bleaching caused by the irreversible binding to the surface. Therefore this peak, which is small regardless, probably does not represent more than one tubulin dimer in the complex. These results indicate that XMAP215 does not create a new species of tubulin oligomer in the polymerization conditions of our assay. If XMAP215 did bind, for example, 5-7 tubulin dimers, these oligomers would be clearly distinguishable from the surface-bound tubulin dimers. We do not observe such oligomers.

5 The E-hook of tubulin mediates the interaction of XMAP215 with microtubules

The far C-termini of tubulin proteins, known as the "E-hooks," are the terminal 12-25 amino acids of alpha and beta tubulins. The E-hooks are comprised of a large number of glutamic acid residues (E), hence the name, that carry a net negative charge. It is presumed to be a flexible region, as it does not appear in tubulin crystal structures. The E-hook has been demonstrated to play a significant role in the interaction of MAPs, motor proteins, and other complexes with the microtubule. The diffusion of MCAK is thought to occur through weak electrostatic interactions between the positively-charged "neck" of MCAK and negative E-hooks of the microtubule (Helenius et al., 2006). To test for a role of the E-hook in the mechanism of XMAP215, we repeated our experiments using microtubule seeds treated with subtilisin, a bacterial protease that specifically removes the E-hook. Subtilisin-digested microtubules and control microtubules were prepared in the same field of view as described previously (Helenius et al., 2006). Figure S7 shows the two types of microtubules and their interaction with 5 nM XMAP215-GFP. The interaction of XMAP215 is substantially reduced on the subtilisin-digested microtubules, although limited lattice and plus-end binding is still observable. This demonstrates that the E-hook is the tubulin domain primarily responsible for XMAP215's lattice interactions.

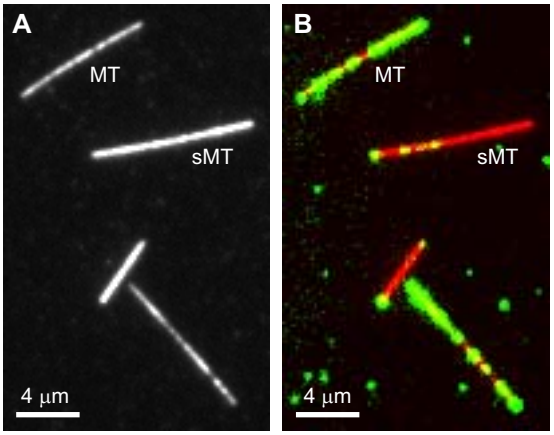

Figure S7: **The interaction of XMAP215 depends on the E-hook of tubulin.** (A) Two types of microtubules are prepared: normal microtubules (MT, dim) and subtilisin digested microtubules (sMT, bright). (B) Dual-color image of normal microtubules (MT) and subtilisin-digested microtubules (sMT) in the presence of 5 nM XMAP215-GFP (green).

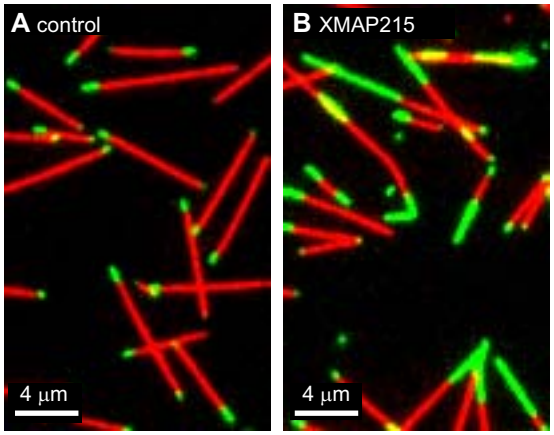

Figure S8: **XMAP215 promotes the growth of GMPCPP tubulin.** Rhodamine-labeled, GMPCPP-stabilized microtubule seeds were adhered to the coverglass (red), and 0.5 μM Alexa Fluor 488-labeled GMPCPP-tubulin (green)was perfused into the chamber. (A) In the absence of XMAP215, very little growth occurs, with a growth rate of 0.07 $\pm$ 0.003 μm·min^{-1}. (B) In the presence of 20 nM XMAP215, the growth rate is 0.3 $\pm$ 0.02 μm·min^{-1}.

6 Role of GTP hydrolysis in microtubule polymerization by XMAP215

We performed a microtubule growth assay using the non-hydrolyzable analog of GTP: GMPCPP. Microtubule seeds were immobilized as in Figure 1 (see Methods), and 0.5 μM GMPCPP-tubulin plus 20 nM XMAP215 were perfused into the reaction chamber. As shown in Figure S8, XMAP215 does accelerate the growth of GMPCPP-tubulin over control experiments without added XMAP215. This demonstrates that XMAP215 does not require GTP hydrolysis in order to increase the association rate of tubulin to the microtubule end. The growth rates under these conditions were 0.30 $\pm$ 0.02 μm·min^{-1} (8.8 dimers·s^{-1}) in the presence of XMAP215 (mean $\pm$ SEM, $n = 54$) and 0.07 $\pm$ 0.003 μm·min^{-1} (2.0 dimers·s^{-1}) in the absence of XMAP215 (mean $\pm$ SEM, $n = 40$). Thus, XMAP215 accelerates the polymerization of GMPCPP-tubulin by a similar factor (fivefold) by which it accelerates polymerization of GTP-tubulin

7 Discussion of models

7.1 Acceleration of growth: the reaction rate perspective

To what extent does XMAP215 accelerate microtubule growth? In the TIRF assay, the peak microtubule growth rates recorded are $\simeq$4 μm·min^{-1} at 5 μM tubulin in the presence of 200 nM XMAP215. As described in Supplementary Information 2, a growth rate of 4 μm·min^{-1} corresponds to the addition of 110 dimers·s^{-1} to the plus end of a 13 protofilament microtubule. We measured an association rate constant, $k_{\rm a}$ = 20 μM^{-1}·s^{-1} to microtubule plus ends. Compare this to the rate constant for tubulin alone: $k_{\rm a}$ = 4 μM^{-1}·s^{-1} to microtubule plus ends (see Figure S2), XMAP215 is increasing the association rate constant by fivefold.

In order to understand how XMAP215 increases the association rate constant, we considered microtubule growth from the point of view of each protofilament. If the microtubule as a whole grows by 110 dimers·s^{-1}, each protofilament grows by only 8.5 dimers·s^{-1}. Therefore, from the point of view of each protofilament, the association rate constant is much lower: $k_{\rm a}^{\rm PF} = 20/13 \simeq 1.5$ μM^{-1}·s^{-1} to protofilament plus ends in the presence of XMAP215 and $k_{\rm a}^{\rm PF} = 0.3$ μM^{-1}·s^{-1} to protofilament plus ends in the absence of XMAP215.

It is important to place these values in the context of other biochemical reactions. Northrup and Erickson used computational techniques to deduce 2-5 μM^{-1}·s^{-1} as the generic upper limit for 3D diffusion limited reaction rate constants between proteins (Northrup and Erickson, 1992). Compare this to the unstimulated association rate constant for tubulin: $k_{\rm a}^{\rm PF} = 0.31$ μM^{-1}·s^{-1}. The implication of this comparison is that microtubule growth is slow: tubulin collides with the protofilament ends much more often than it binds and becomes incorporated into the microtubule lattice.

Our model is that XMAP215 converts more of the collisions of tubulin with the microtubule end into associations of tubulin into the microtubule polymer. In this view, the collision-complexes between tubulin and the microtubule end are unstable, and the tubulin quickly diffuses away. XMAP215 stabilizes these collision complexes, leading to the association of the tubulin into the microtubule polymer.

Importantly, in the presence of XMAP215, the value of $k_{\rm a}^{\rm PF} = 1.5$ μM^{-1}·s^{-1} is within the range for diffusion-limited rate constants of protein-protein associations. In other words, XMAP215 makes things fast, but not that fast. The XMAP215-stiumlated association rate constant to protofilament ends is still below the diffusion limit as calculated by Northrup and Erickson. If XMAP215 increased the association rate constant of tubulin beyond the diffusion-limited rate constant, our model would be inadequate, as we assume the rate constant for the formation of collision complexes is the same with or without XMAP215.

Consider, for example, the association rate constant for MCAK with protofilament ends: $k_{\rm a}^{\rm PF} = 50$ μM^{-1}·s^{-1}. MCAK acheives an association rate constant above the diffusion-limited rate constant because its association is accelerated by a lattice-diffusion targeting mechanism (Helenius et al., 2006).

7.2 Tubulin shuttle model

One aspect of the tubulin shuttle model is that it makes clear predictions for the behavior of XMAP215 at microtubule ends. The model proposes that XMAP215 first binds to several tubulin dimers in solution, targets the ends of the microtubule, attaches the tubulin it carries, and detaches. The first premise of this model, the binding of multiple tubulin dimers, was shown to be false by results described here that demonstrate XMAP215 binds a single tubulin dimer. However, it is possible that "shuttling" of this single tubulin dimer is the mechanism of XMAP215. This would correspond to the "loading" model proposed for Stu2p (Al-Bassam et al., 2006). Therefore, the next question for the model is: can XMAP215 deliver tubulin fast enough to account for the observed growth rates? More specifically, does the flux of XMAP215 to the end equate with the rate of tubulin dimer addition? If too few XMAP215s are arriving, we know that the shuttle model is not sufficient to account for the growth rate.

7.2.1 Flux of XMAP215 to the microtubule end

In order to calculate the flux of XMAP215 to the microtubule end, we use a mass transfer differential equation model, which was previously published by Helenius et al., 2006. The simplified model treats the microtubule end as an infinite sink for the absorption of XMAP215 molecules, in order to calculate the flux of XMAP215 molecules to the microtubule end, regardless of the behavior of XMAP215 upon reaching the end. If $c(x,t)$ is the concentration of XMAP215 on the microtubule lattice at position x from the microtubule end and time t, when we expect that $c(x,t)$ obeys the mass transfer equation:

$$\frac{\partial c}{\partial t} = k_{\rm on} C_{\rm m} - k_{\rm off} c + D\frac{\partial^2 c}{\partial x^2} + v^+ \frac{\partial c}{\partial x} \qquad \text{(S4)}$$

where $k_{\rm on}$ is the attachment rate constant to the microtubule lattice, $k_{\rm off}$ is the dissociation rate constant from the lattice, $C_{\rm m}$ is the XMAP215 concentration in solution, D is the diffusion coefficient on the microtubule lattice, and v^+ is the polymerization rate (Fig. S5).

We specify the following boundary conditions:
(a) $c(x=0) = 0$(infinite sink at the microtubule end),
(b) $c(x\to\infty) = k_{\rm on}C_{\rm m}/k_{\rm off} = c_\infty$,
(c) $\partial c/\partial t = 0$ (steady state assumption).

Table S2: **Parameters for the mass transfer model.**

k_{on}	on-rate constant to the lattice	0.1 ± 0.05 nM^{-1}s^{-1} μm^{-1}
k_{off}	off-rate constant from the lattice	0.41 s^{-1}
D	1D diffusion coefficient	0.30 μm^2 s^{-1}

We also assume a negligible speed for v^+ (in μm·s^{-1}). Then, the mass transfer equation has the solution:

$$c(x) = c_\infty \left(1 - e^{-x/x_0}\right) \tag{S5}$$

where $x_0 = \sqrt{D/k_{\text{off}}}$. From this equation, we can calculate the flux, J, using Fick's first equation, $J = -D \cdot \partial c/\partial x$. At $x = 0$,

$$J_0 = -Dc_\infty/x_0 \tag{S6}$$

Therefore, to calculate the flux to the end, we must measure D, k_{off}, and c_∞. The value of D is 0.30 μm^2 s^{-1}, and k_{off} is the inverse of the mean interaction time with the lattice ($\langle t \rangle^{-1} = 0.41$ s^{-1}). The value of c_∞ can be measured for XMAP215 concentrations of 0.3-3 nM by direct counting of particles. This allowed us to calculate the attachment rate constant to the microtubule lattice, $k_{\text{on}} = 0.1 \pm 0.05$ nM^{-1} s^{-1} μm^{-1}.

With this value of k_{on} and using Eq. S6, we calculated a flux to the end of the microtubule of XMAP215. The measured parameters are summarized in Table S2. We will take the test case of 100 nM XMAP215 with 5 μM tubulin (the conditions used in our experiments). The calculated flux is $J_0 \simeq 8.5$ XMAP215·s^{-1}. The rate of tubulin addition is 82 dimers·s^{-1} (growth rate = 3 μm·min^{-1}). In other words, the flux of XMAP215 to the microtubule end is 9.6× lower than the rate of tubulin addition. Each XMAP215 would need to carry 10 tubulin dimers in order to shuttle sufficient quantities of tubulin. As mentioned previously, our measurements indicate that XMAP215 does not carry 10 tubulin dimers, but rather only one.

7.2.2 End residence

In order for the shuttle model to be correct, a second rate requirement must be met: XMAP215 must detach from the end fast enough to make room for the next XMAP215 add another tubulin dimer. We know that each XMAP215 can transport 1 tubulin dimer. In order to deliver 82 dimers/sec, we require a flux of 82 XMAP215/sec. In an ideal situation, 13-14 XMAP215 molecules would each choose their own protofilaments and never interfere with the neighboring XMAP215 molecules.

In this circumstance, each XMAP215 would reside at the microtubule end for $\langle t \rangle_{end} = (82/13)^{-1} \simeq 0.15$ seconds. If it stayed longer, it would inhibit the next XMAP215 from taking its place at the microtubule end, and we would observe slower growth rates. Therefore, if we observe end-residence substantially longer than 0.15 seconds, we know that XMAP215 must be doing something else at the microtubule end.

We measure values of $\langle t \rangle_{end} = 3.8 \pm 0.7$ s. This argues strongly against the shuttle model–the XMAP215 molecules stay attached to the microtubule end for too long. Of course, it is not necessarily true that every XMAP215 would find an open protofilament binding sites easily and that 13 XMAP215's can reside at the end simultaneously without interfering with one another. If any of these statements are not true, then faster cycling is required to deliver the same amount of tubulin to the end. In other words, when our assumptions do not hold, the argument is driven in our favor.

7.3 Catalytic model

7.3.1 Kinetic scheme

As described in Supplementary Information 2.2, the growth of microtubules, meaning the incorporation of tubulin subunits into a microtubule polymer, can be represented thus:

$$\mathrm{T} + \mathrm{T}_n \underset{k_{\text{d}}}{\overset{k_{\text{a}}[\mathrm{T}]}{\rightleftharpoons}} \mathrm{T}_{n+1} \tag{S1}$$

Our model posits the existence of an intermediate state or collision complex in the growth pathway, represented below as $\mathrm{T} \cdot \mathrm{T}_n$.

$$\mathrm{T} + \mathrm{T}_n \underset{k_{-1}}{\overset{k_{+1}[\mathrm{T}]}{\rightleftharpoons}} \mathrm{T} \cdot \mathrm{T}_n \underset{k_{-2}}{\overset{k_{+2}}{\rightleftharpoons}} \mathrm{T}_{n+1} \tag{S7}$$

where k_{+1} is the second-order association rate constant of the intermediate state, k_{-1} is the dissociation rate constant of the intermediate state, and k_{+2} and k_{-2} are the rate constants for the isomerization reaction whereby the collision complex becomes a strongly-bound tubulin. In this view, the formation and collapse of the collision complex is very fast, while the isomerization is slow.

Now, we suppose that XMAP215 binds to the microtubule end and modifies the rate constants of this growth reaction.

$$\mathrm{T} + \mathrm{XT}_n \underset{k'_{-1}}{\overset{k'_{+1}[\mathrm{T}]}{\rightleftharpoons}} \mathrm{XT} \cdot \mathrm{T}_n \underset{k'_{-2}}{\overset{k'_{+2}}{\rightleftharpoons}} \mathrm{XT}_{n+1} \tag{S8}$$

where XT_n represents XMAP215 bound to the end of a microtubule of n tubulin subunits, and the $'$ symbol indicates the XMAP215-modified rate constants. Within this scheme, our hypothesis is that XMAP215 increases the association rate constant (i.e. $K'_1 = k'_{+1}/k'_{-1} > K_1 = k_{+1}/k_{-1}$). For example, the collision complex may form at the same rate, but may be longer lived ($k_{+1} = k'_{+1}$ but $k'_{-1} = 0.2 \cdot k_{-1}$).

Equations S7 and S8 above are linked by the association and dissociation of XMAP215 to and from the various states, creating the reaction matrix shown below.

$$\begin{array}{ccccc} \mathrm{T}+\mathrm{T}_n & \underset{k_{-1}}{\overset{k_{+1}[\mathrm{T}]}{\rightleftharpoons}} & \mathrm{T}\cdot\mathrm{T}_n & \underset{k_{-2}}{\overset{k_{+2}}{\rightleftharpoons}} & \mathrm{T}_{n+1} \\ k_- \Downarrow k_+[\mathrm{X}] & \circlearrowright 1 & k_-' \Downarrow k_+'[\mathrm{X}] & \circlearrowright 2 & k_- \Downarrow k_+[\mathrm{X}] \\ \mathrm{T}+\mathrm{XT}_n & \underset{k_{-1}'}{\overset{k_{+1}'[\mathrm{T}]}{\rightleftharpoons}} & \mathrm{XT}\cdot\mathrm{T}_n & \underset{k_{-2}'}{\overset{k_{+2}'}{\rightleftharpoons}} & \mathrm{XT}_{n+1} \end{array} \tag{S9}$$

If there are no external energy sources (e.g. if T represents GMPCPP-tubulin), the linkage within the scheme implies that other rate constants must change in order to satisfy detailed balance. The absence of energy dissipation in cycles 1 and 2 in the scheme implies that:

$$K_1 \cdot K = K_1' \cdot K' \tag{S10}$$

$$K_2 \cdot K' = K_2' \cdot K \tag{S11}$$

where $K_1 = k_{+1}/k_{-1}$, etc., $K = k_+/k_-$, and $K' = k_+'/k_-'$. Multiplying equation S10 by equation S11 and canceling terms gives us:

$$K_1 K_2 = K_1' K_2' \tag{S12}$$

Thus, if XMAP215 increases the first association constant ($K_1' > K_1$), it must decrease the second constant ($K_2' < K_2$). For example, $k_{-2}' = 5 \cdot k_{-2}$ and $k_{+2}' = k_{+2}$.

It can be shown that in the absence of an energy source, if XMAP215 increases the polymerization rate then it must increase the depolymerization rate to the same extent. To solve the scheme, we assume there is a population of growing microtubules with all lengths equally represented, such that $[\mathrm{T}_n]=[\mathrm{T}_{n+1}] = \ldots$ and $[\mathrm{XT}_n]=[\mathrm{XT}_{n+1}] = \ldots$. In the absence of XMAP215 ([X]=0), the growth rate of microtubules, dn/dt is represented as:

$$\frac{dn}{dt} = k_{+1}[\mathrm{T}] - k_{-1} \cdot \alpha = k_{+2} \cdot \alpha - k_{-2} \tag{S13}$$

where $\alpha = [\mathrm{T}\cdot\mathrm{T}_n]/[\mathrm{T}_n]$. Solving for α gives:

$$\alpha = \frac{k_{+1}[\mathrm{T}] + k_{-2}}{k_{-1} + k_{+2}} \tag{S14}$$

The critical concentration is obtained by substituting S14 into S13:

$$T_c = (K_1 K_2)^{-1} \tag{S15}$$

At very high XMAP215 concentrations ([X]$\rightarrow \infty$), a similar analysis applies, and the critical concentration in the presence of XMAP215 is:

$$T_c' = (K_1' K_2')^{-1} \tag{S16}$$

Therefore, given equation S12, it is clear that $T_c = T_c'$. In other words, we predict that the critical concentration should be the same in the presence and absence of XMAP215.

If XMAP215 increases the association constant to the intermediate state, then the affinity for XMAP215 for this state must also increase. This follows from S10:

$$K'/K = K_1'/K_1 \tag{S17}$$

Thus, in the absence of an energy source, XMAP215 must bind more strongly to the intermediate state than it binds to the strongly-bound tubulin at the microtubule end.

A scheme similar to Equation S9 has been used to describe enzyme activation (Segel, 1975, p227). The analogy between the activity of XMAP215 and the activation of an enzyme is the following: the microtubule end is itself viewed as an enzyme which catalyzes the reaction in which a tubulin dimer in solution (the substrate) is converted into a tubulin dimer in the microtubule lattice (the product). XMAP215 is then an activator of this enzyme because it increases the polymerization rate.

Supplementary Reference: Segel, I.H. (1975). *Enzyme kinetics : behavior and analysis of rapid equilibrium and steady state enzyme systems* (New York, Wiley).

7.3.2 Comparison to data

In order to verify that $T_c = T_c'$, we measured the critical concentration using both GMPCPP-tubulin and GTP-tubulin with and without XMAP215.

In the absence of XMAP215, the growth rate of 0.5 μM GMPCPP-tubulin is 2.0 $\pm$ 0.63 dimers$\cdot$s^{-1} Figure S8, mean $\pm$ SD, n = 40). In the absence of tubulin, the shrinkage rate of GMPCPP microtubules is 0.49 $\pm$ 0.12 dimers$\cdot$s^{-1} (Figure 5, mean $\pm$ SE, n=10), which corresponds to the dissociation rate constant. The critical concentration is thus 0.10 $\pm$ 0.03 μM and the association rate constant is 4.9 $\pm$ 2.3 μM$^{-1}\cdot$s^{-1}. In the presence of 20 nM XMAP215, the growth rate of 0.5 μM GMPCPP-tubulin is 8.8 $\pm$ 4.4 dimers$\cdot$s^{-1} (Figure S8, mean $\pm$ SD, n=54). In the absence of tubulin, the shrinkage rate of GMPCPP-microtubules is 7.0 $\pm$ 1.2 dimers$\cdot$s^{-1} (Figure 5, mean $\pm$ SD, n=10), which corresponds to the dissociation rate constant. The critical concentration is 0.22 $\pm$ 0.07 μM and the association rate constant is 32 $\pm$ 12 μM$^{-1}\cdot$s^{-1}. Thus, in the presence of 20 nM XMAP215, the critical concentration is relatively unchanged (2.2 $\pm$ 1.1 fold). This change is not statistically significant, given the experimental uncertainties.

In the case of GTP-tubulin, we estimated the critical concentration by extrapolating the growth curves in Figure **S2** back to zero growth (the x-intercept). The critical concentrations are -0.3 $\pm$ 0.8 μM and -0.9 $\pm$ 3.3 μM with and without XMAP215, respectively. Of course, a negative critical concentration is not physically possible, but the

uncertainties imply that the values are not significantly different from zero or from each other. Therefore, our data support the conclusion that $T_c = T_c^{'}$.

7.3.3 Summary

In conclusion, our data are consistent with a kinetic scheme in which XMAP215 stabilizes an intermediate in the polymerization reaction by slowing the dissociation of a collision complex ($k_{-1}^{'} < k_{-1}$) and, by detailed balance, speeding up the formation of the intermediate along the depolymerization pathway ($k_{-2}^{'} > k_{-2}$). Importantly, we expect a similar magnitude increase in both polymerization and depolymerization and that the critical concentration is unchanged. These expectations are met within a factor of two for both GMPCPP-tubulin and GTP-tubulin, and the deviation from the expected behavior is not statistically significant.

8 Detailed methods

8.1 Protein expression details

For XMAP215 expression in insect cells, PCR products including sequences coding His_7 and enhanced green fluorescent protein (EGFP)-His_7 tags from pEGFP-N1 (Clontech) were inserted at the C-terminus of the coding region of XMAP215. XMAP215-His_7 and XMAP215-EGFP-His_7 were cloned into the pFastBac1 vector for the BAC-TO-BAC baculovirus expression system (Invitrogen). *Spodoptera frugiperda* expresSf+ cells expressed XMAP215-His_7 and XMAP215-EGFP-His_7 after infection with virus generated using these plasmids. Cells were pelleted after 54 hrs of infection and resuspended in ice-cold lysis buffer (50 mM HEPES pH 7.5, 50 mM NaCl, 5% glycerol, 0.1% Triton-X-100, 10 U/ml Benzonase and 1x protease inhibitors mix (1 μg/ml AMPSF, 10 μg/ml antipain-HCl, 6 μg/ml chymostatin, 2 μg/ml aprotinin, 0.7 μg/ml pepstatin A, 0.5 μg/ml leupeptin, and 3.6 μg/ml E64). The resuspended cells were homogenized using a Dounce homogenizer. The crude lysate was clarified by centrifugation and loaded onto an SP-sepharose column (HiTrap SP-HP, GE Healthcare) equilibrated with cation buffer (6.7 mM HEPES-/KOH pH 7.5, 6.7 mM MES, 6.7 mM Na-acetate, and 200 mM NaCl). The column was washed with cation buffer, and the protein was eluted from the column with a continuous salt gradient (200 mM-600 mM NaCl) using a BioCAD SPRINT system. Peak fractions were pooled, brought to 15 mM imidazole, and loaded onto a Ni^{2+}-sepharose column (GE Healthcare HisTrap HP) equilibrated with imidazole buffer (50 mM $NaPO_4$ buffer pH 8.0, 300 mM NaCl, 15 mM imidazole, 10% glycerol, 1 mM $MgCl_2$, 10 μM Mg-ATP). The column was washed with 30 mM imidazole and 60 mM imidazole buffers and XMAP215 was eluted with 500 mM imidazole. Peak XMAP215-His_7 fractions were pooled and the buffer exchanged to storage buffer (10 mM Bis-Tris Propane, 10 mM TrisHCl, 330 mM NaCl, 1 mM DTT, 10% glycerol) using a NAP25 desalting column (GE Healthcare). Aliquots of XMAP215-His_7 were flash frozen and stored in liquid N_2. In the case of XMAP215-EGFP-His_7, peak Ni-column fractions were pooled and passed through a size exclusion chromatography column (GE Healthcare Superdex 200 16/60) pre-equilibrated with elution buffer: BRB80 (80 mM PIPES-/KOH pH 6.9, 1 mM $MgCl_2$, 1 mM EGTA), 150 mM KCl, and 1 mM DTT. Only the single peak fraction from the size exclusion chromatography column was used. Most experiments with XMAP215-EGFP-His_7 were performed using freshly purified protein. Protein was stored with glycerol added to 10% in liquid N_2. Protein concentrations were estimated using a Bradford assay (Bio-Rad Protein Assay) and the absorbance at $\lambda = 280$ nm. As initial positive controls, the ability of XMAP215 and XMAP215-GFP to promote microtubule growth was examined using standard fixed-time point assays (data not shown).

8.2 Coverslip silanization

Microscope chambers were constructed using two silanized cover-slips separated by double-stick tape (Scotch 3M) such that channels 0.1 mm thick, 3 mm wide and 18 mm long are formed. Before silanization, 18 mm×18 mm and 22 mm×22 mm cover-slips (no. 1.5, Corning) were extensively cleaned by immersion in different solutions in the following order: 55 min in acetone, 10 min in ethanol, 1 min nano-pure water, 60 min in Pirnaha solution (H_2O_2:H_2SO_4, 3/5), three 1 min water rinses, 0.1 M KOH, and finally two 1 min water rinses before drying in nitrogen. Following 1-hour of silanization in 0.05% dichlorodimethylsilane in trichloroethylene, cover-slips were washed 4 times in methanol while sonicated. After 3 further rinses with nano-pure water, silanized cover-slips were stored dry. The coverslip/doublesided tape sandwich was assembled in cover-slip holders designed to allow imaging through the bottom cover-slip (22 mm×22 mm).

8.3 Size exclusion chromatography

Size exclusion chromatography was carried out using a Tosoh TSK_{gel}G5000PWXL column equilibrated in 25 mM TrisHCl (Roth) pH 7.5, 75 mM NaCl (VWR), 1 mM $MgCl_2$ (VWR), 1 mM EGTA (Sigma), 0.1 % Tween20 (VWR), 1 mM DTT (Fermentas), and 0.2 mM GTP (Sigma). The column was calibrated with standard proteins (General electrics) of known Stokes radii plotted against the common logarithm of their elution volumes. The common logarithm of the elution volumes of XMAP215, tubulin and the XMAP215/tubulin complex were used to determine

their Stokes radii. XMAP215 (5.7 μM) and tubulin (1.43 μM and 14.3 μM) or the equivalent buffer in case of single protein injection were mixed with 1 mM GTP in vitro incubated for 10 min on ice and then injected onto the Tosoh TSK_{gel}G5000PWXL size exclusion column. From the collected fractions (100 μl) 12 μl were mixed with 6x protein sample buffer and 10 μl separated by 4–12 % SDS-PAGE (NuPage, Invitrogen). The SDS-PAGEs were stained with Coomassie brilliant blue R250 (Merck). Standard proteins used in the size exclusion chromatography (Stokes radii are indicated in brackets): ribonuclease A (1.64 nm), chymotrypsinogen (2.09 nm), ovalbumin (3.05 nm), BSA (3.55 nm), aldolase (4.81 nm), catalase (5.22 nm), ferritin (6.1 nm), thyroglobin (8.5 nm).